Research Article

Xuekun Jiang, Zhirong Jia*, Yaoxi Han, Xinyu Yang, Xuejing Wang and Jiantong Wu

Enhancing frost resistance of alkali-activated slag concrete using surfactants: sodium dodecyl sulfate, sodium abietate, and triterpenoid saponins

https://doi.org/10.1515/rams-2025-0176
Received March 31, 2025; accepted October 21, 2025;
published online December 11, 2025

Abstract: To investigate surfactants for enhancing the frost resistance of alkali-activated slag concrete (AASC), three surfactants were selected: Sodium Dodecyl Sulfate (SDS), Sodium Abietate (SA), and Triterpenoid Saponins (TS). The setting time of alkali-activated slag (AAS) was tested at surfactant dosages of 0.01 %, 0.03 %, 0.05 %, 0.07 %, and 0.09 %. The 28 days compressive strength, freeze-thaw resistance (mass loss, relative dynamic modulus of elasticity (RDME), and strength loss after 28 cycles), and water absorption were evaluated. The microstructure was observed using a scanning electron microscope, and the hole structure was analyzed using mercury intrusion porosimeter. The results indicate that all three surfactants reduce the initial setting time and increase the final setting time of AAS. When the dosage of TS is 0.01 %, the mass loss after 20 freeze-thaw cycles is reduced by 39.2 %, the RDME increases by 13.9 %, the water absorption rate is reduced by 50 %, and the compressive strength loss rate is reduced by 55.3 %. The incorporation of TS surfactants increases the number of closed micro-bubbles in the concrete, reduces the most probable hole size and average hole size, and decreases the proportion of large and harmful holes that improved the frost resistance of AASC.

Keywords: surfactants; alkali-activated slag concrete; frost resistance; material properties; microanalysis

1 Introduction

Ordinary Portland cement (OPC) has been widely used in civil engineering due to its good mechanical properties. However, the production of OPC requires a large amount of energy and non-renewable minerals (such as limestone), and the calcination process of limestone at high temperature (1,500 °C) will emit a large amount of CO^2 into the atmosphere [1–4]. In the context of global efforts to reduce carbon emissions and natural resource consumption, alkali-activated materials have attracted the interest of many researchers [5, 6]. After years of research and development, alkali-activated slag (AAS) is a reliable alternative to cement materials. Compared with ordinary Portland cement, AAS has completely different hydration reaction processes [5]. The use of AAS not only reduces the resources needed to produce cement, reduces carbon dioxide emissions, but also effectively consumes industrial solid waste. As a new type of environmentally friendly cementitious material, AAS can not only reduce the burden of the environment and reduce carbon dioxide emissions, but also provide excellent performance, including higher chemical erosion resistance, as well as lower hydration heat and permeability [7–10].

Studies have shown that AAS has high strength and good frost resistance [11, 12]. It can withstand 1,000 freeze-thaw cycles and is suitable for cold regions in the north [13]. Some studies have used X-ray diffraction to analyze the hydration products of AAS. The results show that the internal hole structure of AAS is compact and has outstanding frost resistance and impermeability. X-ray diffraction analysis showed that there was no calcium hydroxide and other substances in the hydration products, which avoided the formation of harmful ettringite by reaction with sulfate [14]. The results showed that with the increase of freeze-thaw cycles, the strength loss rate and RDME loss rate of each group of specimens increased continuously. The loss rate of sodium sulfate group was the highest, followed by sodium chloride group, and the water freezing group was the lowest

***Corresponding author: Zhirong Jia**, School of Civil Engineering and Geomatics, Shandong University of Technology, Zibo, 255000, China, E-mail: jiazhr@126.com. https://orcid.org/0000-0002-2555-5921
Xuekun Jiang, Yaoxi Han, Xinyu Yang, Xuejing Wang and Jiantong Wu, School of Civil Engineering and Geomatics, Shandong University of Technology, Zibo, 255000, China

[15]. However, there is still room for improvement in its frost resistance compared with cement concrete. Therefore, the frost resistance of AAS can be further improved by introducing an appropriate number of surfactants [16–18].

The surfactants help to form tiny bubbles inside the cement concrete, reduce the water condensation pressure inside the concrete, and improve the frost resistance [19]. Scholars at home and abroad have studied the influence of surfactants on the frost resistance of cement concrete. The hole structure characteristics of air-entraining concrete are measured by mercury intrusion porosimeter [20]. The results show that the incorporation of surfactants can improve the frost resistance of cement concrete, and surfactants can increase the cumulative hole volume of cement concrete [21]. Under the appropriate dosage of surfactants, the cement particles can be better dispersed in water, and the degree of hydration of cement can be improved. In addition, small bubbles with uniform distribution can be introduced into concrete, so as to improve the frost resistance of cement concrete. However, the incorporation of surfactants increases the porosity of cement concrete, resulting in a decrease in its mechanical properties, which is greatly affected by the size and distribution of holes in cement concrete [22–26].

A large number of chemicals can be used as surfactants for concrete [27–29]. Many of these are by-products of various industrial processes, such as pulp, paper, and oil production. At present, the commonly used surfactants include: rosin resin, such as rosin thermal polymer, rosin soap, etc.; alkyl and alkyl aromatic sulfonic acids, such as SDS, sodium dodecyl benzene sulfonate, sodium dodecyl alcohol ether sulfate, etc.; fatty alcohol sulfonates, such as fatty acid polyoxymethylene ether sodium sulfate; saponins, such as TS [28, 30]. Studies have shown that SDS not only has strong foaming ability, but also has low cost and is suitable as a foaming material in a foaming agent [31]. The optimum foaming mass concentration is 4 g/L. On the whole, the half-life of SDS foam is very short, the stirred foam is not stable, the half-life is only about 6 min, and the foam is completely eliminated about 1 h [32]. Other studies have shown that sodium abietate, as an admixture of concrete, greatly improves the mechanical properties of high-strength concrete. It not only has low cost, but also provides a simple and easy construction process [33]. Under the same water-cement ratio, the impermeability of concrete with sodium abietic acid surfactants is higher than that of concrete without sodium abietic acid surfactants, and when the air content is 5 %, its strength not only does not decrease but also increases, but the air content is too high. It will also lead to a sharp decline in the frost resistance of concrete. Under the condition of freeze-thaw cycle, compared with the compressive strength of zero content concrete, with the increase of sodium abietate surfactants content in the corresponding age has improved significantly, showing a positive correlation [34]. In addition, sodium abietate, as a surfactant, introduces a large number of discontinuous, tiny and closed bubbles at a suitable dosage, which can improve the workability of mortar to a certain extent, and improve the hole distribution during early freezing, and resist the frost heaving stress caused by the freezing of unhydrated part of water, but the improvement of hydration process of other cementitious materials such as cement is not great [35]. Studies have shown that the mortar of triterpenoid saponins has better bubble retention ability and better air-entraining effect [36]. This is because the non-ionic air-entraining admixture does not precipitate calcium ions in cement hydrates. The effect and bubble retention performance are better than the two anionic surfactants [37, 38]. Other studies have shown that the small amount of triterpenoid saponins surfactants can significantly improve the performance of concrete. Other studies have shown that small dosage of triterpenoid saponins surfactants can significantly improve the performance of concrete. When the air content is less than 3 %, the compressive strength of concrete increases slightly. The strength of concrete decreases with the increase of air content. When the air content of concrete is 3 %–6 %, the frost resistance and impermeability are obviously improved. When the air content of triterpenoid saponin surfactants is 5.5 %, the number of freeze-thaw cycles is more than 300 times, the RDME of concrete after 300 freeze-thaw cycles is 90 %, and the mass loss rate is 0.4 % [39, 40]. No matter the curing conditions or alkali activator, hybrid alkali activated mortars with a high concentration of GBFS have better compressive strength at both young and old ages. This may be because GGBFS has a high concentration of CaO and glassy properties, which make it easier to create C-A-S-H gels, which reduce porosity while enhancing microstructure. By plugging the permeable voids and micro cracks with 10 % clinker content, the sorptivity, porosity, and water absorption were decreased. An increase in calcium and a decrease in alumina and silica caused by a higher clinker content of 30 % led to a substantially weaker geopolymer matrix and enhanced permeability, which affected durability [41, 42].

These results indicate that the effects and mechanisms of surfactants on AASC require further investigation. Currently, the research on the frost resistance of AASC incorporating surfactants still faces the following issues:

1) What is the effect of common surfactants on the setting time and mechanical properties of AASC.
2) What is the effect of common surfactants on the frost resistance of AASC.
3) What is the mechanism of action of surfactants in AASC.

To solve the above problems, three kinds of surfactants, SDS, SA and TS were selected to research the effect of different

dosage on the setting time and mechanical properties of AASC. The microstructure and hydration products of AASC under different conditions were observed by SEM, and the reaction mechanism was explained. The purpose of this study is to select an effective admixture that can significantly improve the frost resistance of alkali-activated slag concrete from three surfactants, and to determine the optimal dosage of the selected admixture.

2 Materials and methods

2.1 Raw material

2.1.1 Slag

The slag was produced by Fuheng Mineral Products Trade Co., Ltd., and the chemical composition is shown in Table 1.

2.1.2 Alkali activator

The water glass was purchased from Henan Platinum New Material Co., Ltd., white powder, modulus is 2.02. The sodium hydroxide was purchased from Shandong Puhui Fen Chemical Technology Co., Ltd., with a content ≥96 %.

2.1.3 Surfactants

SDS was purchased from Tianjin Zhiyuan Chemical Reagent Co., Ltd., SA from Jinan Chaoyixing Chemical Co., Ltd., TS from Jinan Shunxin Chemical Co., Ltd. SDS is an organic compound, a pale-yellow solid, needle-like. SA is a white powder with a content of 99.12 %, an activity value of 79, dissolved as a colorless clear liquid, impurities ≤0.1 %, petroleum ether soluble ≤2.5 %, inorganic salt content ≤7.5 %, pH value ≥ 10.0. TS is light-yellow powder, the water reduction rate is 6.5 %, the gas content is 3.5 %, the bleeding ratio is 80 %, and the chloride ion content is ≤ 1 %.

2.1.4 Aggregate

The aggregate was purchased from Shandong Dongcheng Building Materials Company. The coarse aggregate is natural stone with a particle size range of 5–20 mm, and the fine aggregate is river sand with a particle size range of 0–4.75 mm.

2.2 Experimental design

2.2.1 Test groups

The precursor is slag, the activator is composed of water glass and sodium hydroxide, modulus is 1, and the content is 4 %. The dosages of SDS, SA and TS are 0.01 %, 0.03 %, 0.05 %, 0.07 % and 0.09 %. Test ranges were selected based on preliminary studies [39, 41]. The preparation and test flow chart of AASC is shown in Figure 1, the testing groups are showed in Table 2.

2.2.2 Water-binder ratio

The standard consistency test was carried out to determine the optimal water consumption according to the *Highway Engineering Cement and Cement Concrete Test Procedures* (JTG 3420-2020), the water-binder ratio (w/b) was fixed at 0.4.

2.2.3 Sample curing

The AASC samples were first placed into a standard curing box and maintained for 24 h before demolding. Following demolding, the samples were sequentially transferred to a curing room for further conditioning. During this process, the water level in the curing environment was carefully controlled to be 2 cm above the top surface of the specimens. The curing room was maintained at a temperature of 20 ± 1 °C with a relative humidity exceeding 90 % according to JTG 3420-2020.

2.3 Test method

2.3.1 Setting time

The standard consistency was established first. The activator and surfactants were dissolved in water beforehand. Next, the slag and solution were added to the mixing pot, and the time was noted. Simultaneously, the mixture was stirred slowly for 120 s, paused for 15 s, and then stirred quickly for

Table 1: Chemical composition of slag.

Oxides	CaO	Al_2O_3	SiO_2	MgO	Fe_2O_3	TiO_2	SO_3	MnO	Na_2O
Mass (%)	42.6	14.2	27.8	8.09	0.378	1.2	2.46	0.401	0.55

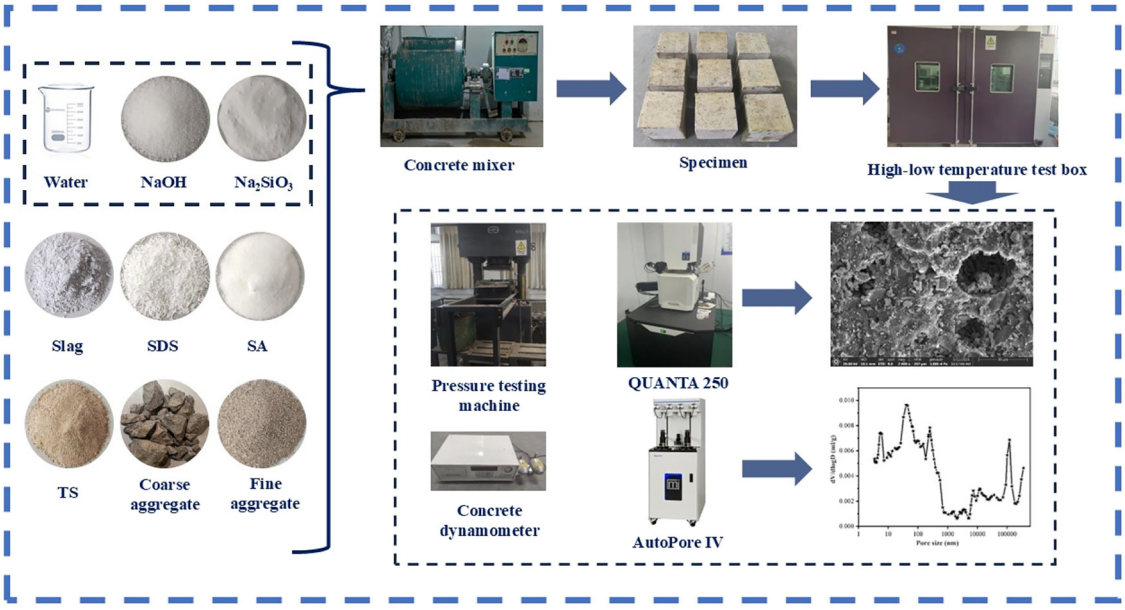

Figure 1: The preparation and test flow chart of AASC.

Table 2: Testing groups.

Mix Id	Surfactant dosages (%)
M0	0
SDS1	0.01
SDS2	0.03
SDS3	0.05
SDS4	0.07
SDS5	0.09
SA1	0.01
SA2	0.03
SA3	0.05
SA4	0.07
SA5	0.09
TS1	0.01
TS2	0.03
TS3	0.05
TS4	0.07
TS5	0.09

another 120 s. After mixing, the initial and final setting times were measured at intervals of 15 min or less according to JTG 3420-2020.

2.3.2 Compressive strength

Retrieve the specimen from the curing chamber and cover it with a damp cloth. Position the test piece on the lower platen of the testing machine and align it geometrically. As the specimen nears failure and starts to deform rapidly, halt the machine's accelerator until failure occurs, and record the ultimate load. Calculate the average of the measured values from three specimens to obtain the final result, rounded to 0.1 MPa. If the difference between the highest or lowest value and the median value exceeds 15 % of the median, the median value will be used as the measured result. If both the highest and lowest values deviate from the median by more than 15 %, the test results for that group are considered invalid according to JTG 3420-2020.

2.3.3 Freeze-thaw cycle test

During the curing period from Day 2 to Day 7, four surfaces perpendicular to the test surface were sealed with epoxy resin. Throughout the sealing process, the specimen was kept clean and dry, and its mass was measured and recorded both before and after sealing. The sealed specimen was then placed in a specimen box with the test surface facing downward, resting on a spacer. A non-metallic triangular spacer or support, 5 mm in height and resistant to water absorption and deformation, was also placed in the box. When a 3 % NaCl solution was added to the box, care was taken to prevent the specimen's top surface from being splashed. The liquid level was maintained at 10 ± 1 mm above the specimen. After adding the solution, the specimen was pre-saturated for 7 days at a temperature of 20 ± 2 °C.

Once pre-saturation was complete, the initial value of the transverse fundamental frequency was measured using a dynamic elastic instrument. After measurement, the specimen was repositioned in the box. The temperature was

then set according to a prescribed freeze-thaw cycle system, and the test chamber was opened once the settings were confirmed. In the single-sided freeze-thaw test, the freeze-thaw cycle was not interrupted. The mass of spalling material, the specimen's mass, and its dynamic elastic modulus were measured every four freeze-thaw cycles according to *Standard for test methods of long-term performance and durability of concrete* (GB/T 50082-2024).

When one of the following conditions occurs in the freeze-thaw cycle, the test can be stopped:

1) When reaching 28 freeze-thaw cycles?
2) When the spalling amount per unit area of the specimen is greater than 1.5 kg/m^2?
3) When the RDME of the specimen is reduced to 80 %?

2.3.4 Micro-analysis

The microstructure and chemical composition were analyzed by SEM. The instrument used is QUANTAFEG250 field emission scanning electron microscope produced by FEI company in the United States. Before SEM-EDS analysis, the selected samples were soaked in anhydrous ethanol for 7 days, so that the hydration reaction was completely stopped.

2.3.5 MIP

The instrument used was the AutoHole IV 9500 high-performance automatic mercury injection machine produced by McMuritik in the United States. The mercury intrusion test samples were taken from the fragments after the mechanical property test, immersed in anhydrous ethanol for 7 days to terminate the hydration, and then dried in a vacuum drying oven for 24 h before the mercury intrusion test.

3 Result and discussion

3.1 Setting time

In Figure 2, it can be seen that the incorporation of all surfactants reduce the initial setting time and prolong the final setting time to a certain extent compared with the group without surfactants. There is little difference between different amounts of surfactants, which indicates that the incorporation of surfactants has little effect on the setting time of AAS.

From Figure 2(a), the addition of SDS reduces the initial setting time of AAS and prolongs the final setting time. Compared with M0, when the content of SDS is 0.05 %, the initial setting time decreases the most, which is 38.5 %, and the final setting time increases the least, which is 24.4 %. When the content of SDS is 0.01 %, the initial setting time is reduced by 28.2 %, and the final setting time is increased by 27.7 %.

From Figure 2(b), the addition of SA reduced the initial setting time and increased the final setting time, but compared with SDS, the initial setting time was reduced. Compared with M0, when the content of SA is 0.01 %, the initial setting time decreases the most, which is 53.8 %. When the content is 0.03 %, the final setting time prolongs the least, which is 23.9 %. When the content is 0.07 %, the initial setting time decreases the least, which is 43.6 %. When the content is 0.05 %, the final setting time prolongs the most, which is 28.6 %.

From Figure 2(c), the addition of TS reduced the initial setting time and prolongs the final setting time. Compared with M0, when the content of TS was 0.05 %, the initial setting time decreased the most, which was 51.3 %, and when the content was 0.09 %, the initial setting time decreased the least, which was 33.3 %. When the dosage is 0.03 %, the final setting time prolongs the most, which is 29.6 %. When the dosage is 0.07 %, the final setting time prolongs the least, which is 26.3 %.

3.2 Unit area peeling amount

The single-sided freeze-thaw test was carried out on AASC with different surfactants. The experimental data are shown in Figure 3.

From Figure 3, with the increase of the number of freeze-thaw cycles, the amount of peeling per unit area showed an upward trend. Compared with the M0 group, except for 0.09 % SA, the mass loss of AASC mixed with surfactants decreased to varying degrees. Among them, the AASC with TS surfactants has the smallest mass loss, followed by SDS, and SA is the largest. It can be seen that TS has the best effect on the reduction of AASC mass loss, and SA has the worst effect.

From Figure 3(a), the mass loss of AASC decreased first and then increased with the increase of SDS content. When the content of SDS was 0.07 %, the mass loss was the lowest. In the SDS4 group, the mass loss of 24 freeze-thaw cycles was 1.33 kg/m^2, which was 0.2 kg/m^2 lower than that of M0 (1.53 kg/m^2) and decreased by 13.07 %. The mass loss of 24 freeze-thaw cycles was 1.33 kg/m^2, which was lower than that of M0 (20 freeze-thaw cycles). However, when the content of SDS increased to 0.09 %, the mass loss of AASC began to increase, but it was still lower than that of M0 group.

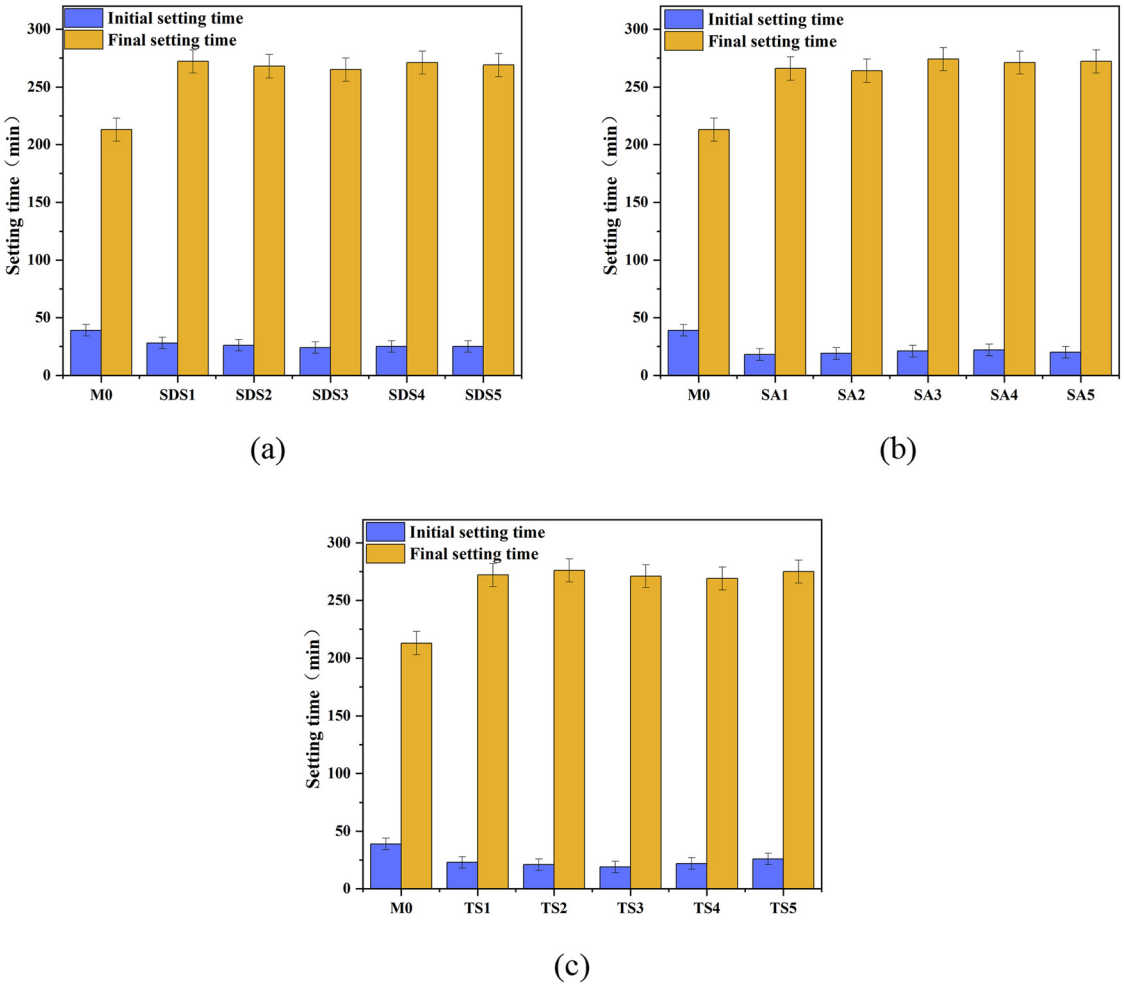

Figure 2: The setting time of AAS with surfactants.

From Figure 3(b), the mass loss of AASC decreased first and then increased with the increase of SA content. When the content of SA was 0.05 %, the mass loss of AASC was the lowest. In the SA3 group, the mass loss of 20 freeze-thaw cycles was 1.48 kg/m^2, which was 0.05 kg/m^2 lower than that of the M0 group, a decrease of 3.27 %. When the content of SA was 0.09 %, the mass loss of AASC increased rapidly, and the mass loss of 16 freeze-thaw cycles reached 1.96 kg/m^2, which was much higher than that of M0 group.

From Figure 3(c), with the increase of TS surfactants content, the spalling amount per unit area of AASC decreases first and then increases. When the TS content is 0.01 %, the mass loss of AASC is the least, and the mass loss after 20 cycles is 0.93 kg/m^2, which is lower than the mass loss of 20 freeze-thaw cycles in M0 group, which is reduced by 0.6 kg/m^2 and reduced by 39.22 %. When the content of TS is higher than 0.01 %, the effect becomes worse, and the mass loss of AASC begins to increase. When the content is 0.09 %, it reaches the highest, but it is lower than the mass loss of M0 group.

3.3 Relative dynamic modulus of elasticity

The RDME can measure the propagation velocity of elastic waves in concrete. After the freeze-thaw cycles, the internal structure of AASC is destroyed, and the dynamic elastic modulus will also change. RDME is one of the important indexes to evaluate the frost resistance of AASC. Draw the test data into a line chart, as shown in Figure 4.

From Figure 4(a), the RDME of all groups gradually decreases with the increase of the number of freeze-thaw cycles. The RDME of SDS1, SDS2, SDS3, SDS4 and SDS5 decreased to 78.9 %, 81.3 %, 81.9 %, 86.0 % and 79.2 % respectively after 20 freeze-thaw cycles, which was higher than that of M0 (77.0 %). Compared with the M0 group, the relative elastic

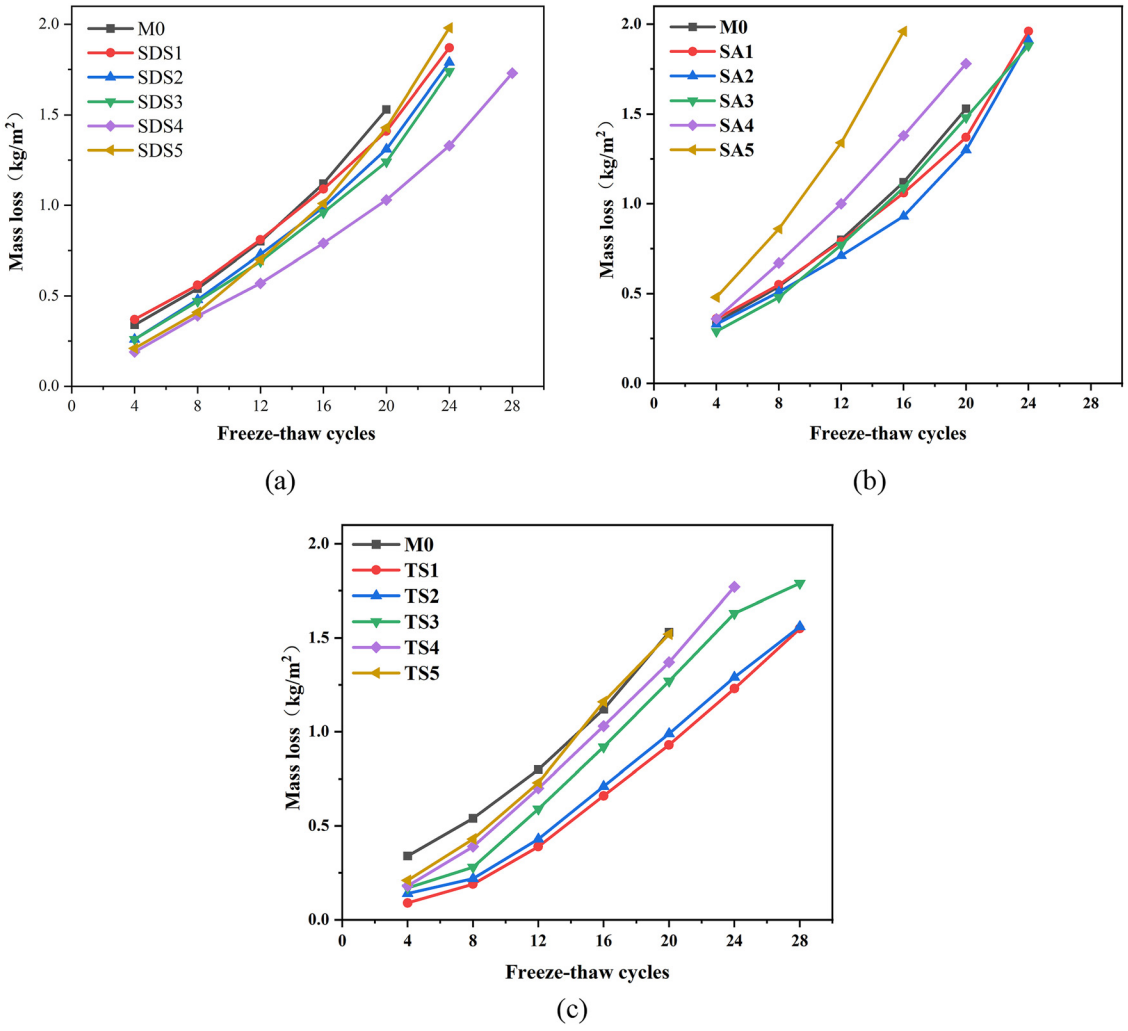

Figure 3: Mass loss of concrete under different freeze-thaw cycles.

modulus of AASC increased first and then decreased with the increase of SDS content. When the content of SDS is 0.07 %, the RDME of AASC is the highest.

From Figure 4(b), when the freeze-thaw cycle reached 20 times, the RDME of SA1, SA2, SA3 and SA4 were 80.2 %, 82.1 %, 82.8 % and 75.7 %, respectively. The RDME of SA5 decreased to 71.9 % after 16 freeze-thaw cycles. It can be seen that the RDME increases first and then decreases with the increase of SA content. When the SA content is less than 0.05 %, the loss of dynamic elastic modulus of AASC undergoing multiple freeze-thaw cycles can be reduced. When the content is 0.07 %–0.09 %, the RDME of AASC mixed with SA decreases more than that of M0 group, indicating that the excessive incorporation of SA will have a negative impact on the frost resistance of AASC.

From Figure 4(c), the RDME of TS1, TS2 and TS3 were 77.8 %, 76.6 % and 73.2 %, respectively, when the freeze-thaw cycle was 28 times. When the number of freeze-thaw cycles is 24, the RDME of TS4 is 74.4 %; when the number of freeze-thaw cycles is 20, the RDME of TS5 is 80.3 %. It can be seen that the RDME increases first and then decreases with the increase of TS content. When the TS content is less than 0.05 %, the frost resistance of AASC can be significantly improved and the loss of dynamic elastic modulus can be reduced. When the content is 0.01 %, the effect is the best.

3.4 Strength loss rate

The compressive strength and loss rate test data of AASC mixed with different surfactants before and after freeze-thaw cycles were plotted, as shown in Figures 5 and 6.

From Figure 5, when there are no freeze-thaw cycles, the higher the number of surfactants, the greater the negative impact on the compressive strength of AASC28d. When the content is 0.01 %, the 28d compressive strength of AASC

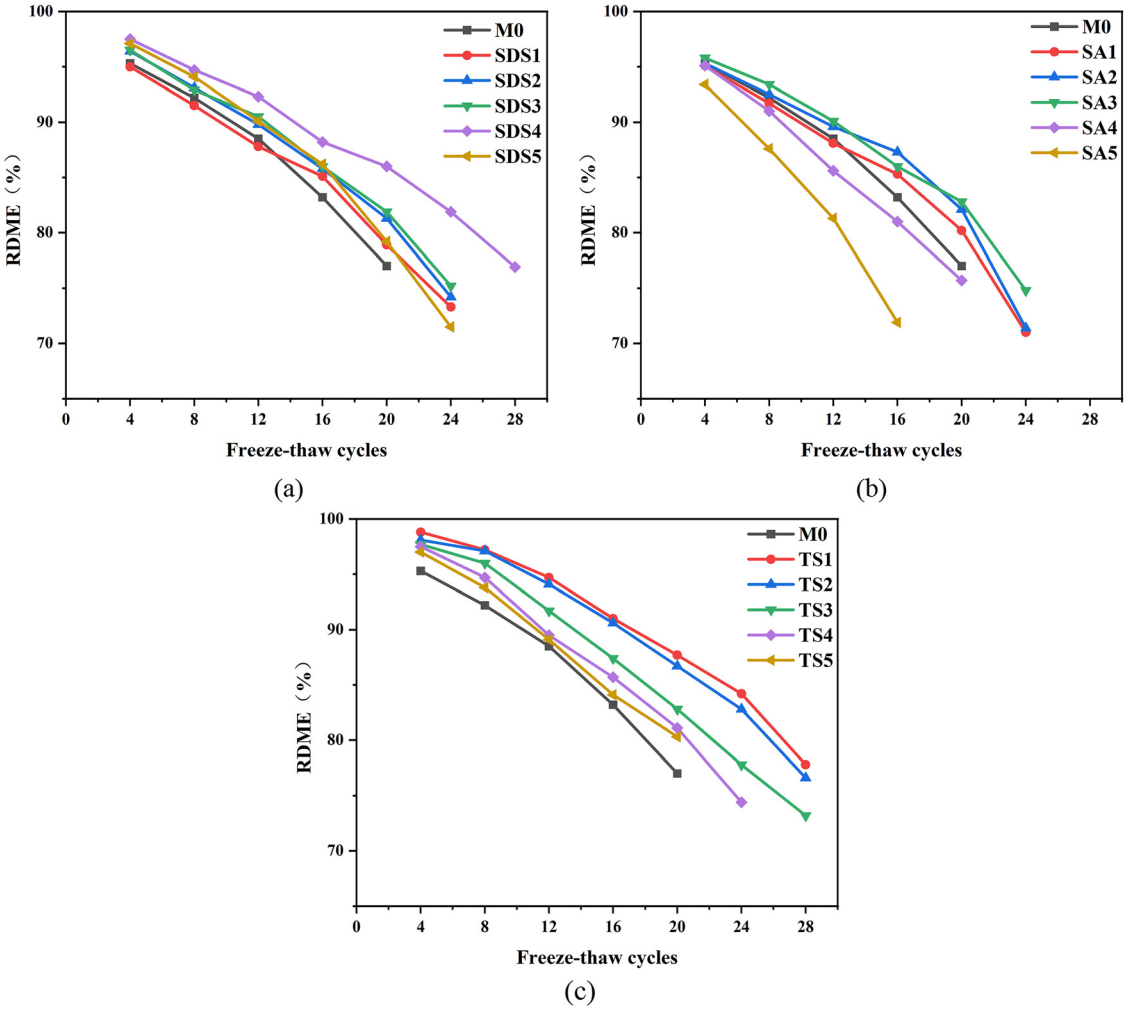

Figure 4: Relative dynamic modulus of elastic under different freeze-thaw cycles.

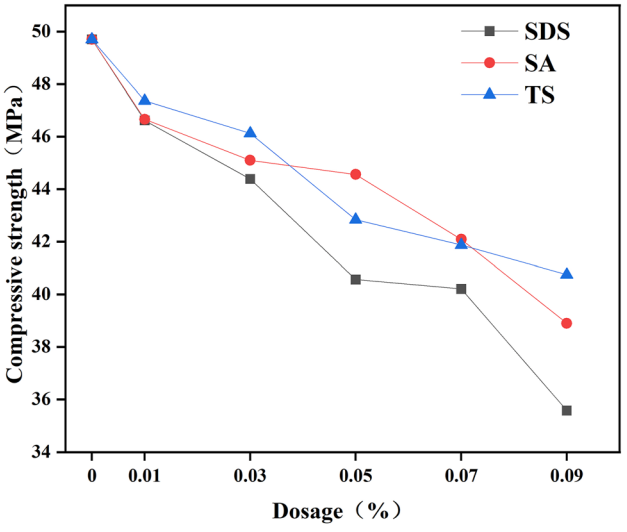

Figure 5: Compressive strength at 28d.

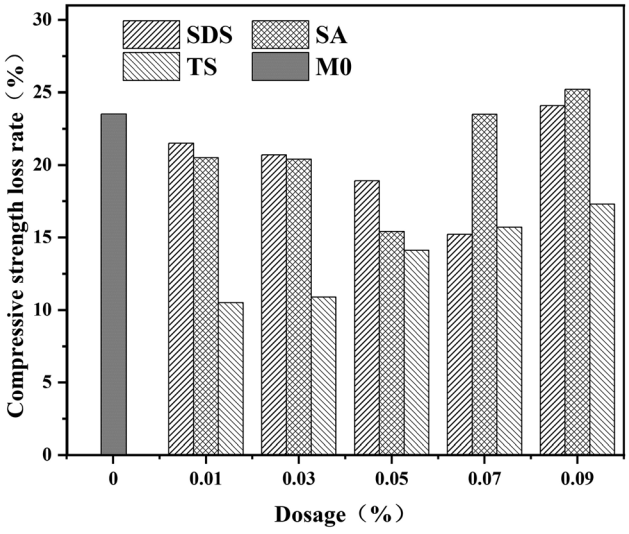

Figure 6: Compressive strength loss rate.

decreases slightly. The 28d compressive strength of AASC mixed with SDS, SA and TS are 3.1 MPa, 3 MPa and 2.3 MPa lower than that of M0 group, and 6.2 %, 6 % and 4.6 % lower than that of M0 group. When the content of SDS was 0.03 %, 0.05 %, 0.07 % and 0.09 %, the 28d compressive strength decreased by 10.7 %, 18.3 %, 19.1 % and 28.4 % respectively. When the SDS content is 0.09 %, the 28d compressive strength is the smallest, which is 35.6 MPa. When the content of SA was 0.03 %, 0.05 %, 0.07 % and 0.09 %, the 28d compressive strength decreased by 9.3 %, 10.5 %, 15.3 % and 21.7 % respectively. It can be seen that the SA content is less than 0.05 %, which has little negative effect on the 28d compressive strength of AASC. When the content is 0.05 %–0.09 %, the loss of 28d compressive strength increases. When the content of TS was 0.01 %, 0.03 %, 0.05 %, 0.07 % and 0.09 %, the 28d compressive strength decreased by 4.6 %, 7.2 %, 13.9 %, 16 % and 17.9 %. It can be seen that TS has the least negative effect on the 28d compressive strength of AASC, and SDS has the greatest negative effect on the 28d compressive strength. This is because the incorporation of surfactants makes the air content in AASC increase, and the relative density of AASC decreases, resulting in a decrease in compressive strength.

From Figure 6, the compressive strength loss rate of AASC decreases first and then increases with the increase of SDS content. When the SDS content is 0.07 %, the compressive strength loss rate is the lowest, which is 15.2 %. With the increase of SA content, the compressive strength loss rate of AASC increases first and then decreases. When the SA content is 0.05 %, the compressive strength loss rate is the smallest, which is 15.4 %. The compressive strength loss rate of AASC increases with the increase of TS content. When the TS content is 0.01 %, the compressive strength loss rate is the lowest, which is 10.5 %. The results show that the incorporation of TS in the three surfactants can significantly reduce the compressive strength loss of AASC after freeze-thaw, followed by SDS, and finally SA. In addition, it should be noted that the incorporation of excessive SDS and SA will not reduce the loss of compressive strength, but will lead to an increase in the loss of compressive strength.

3.5 Water absorption rate

The experimental data of the effect of surfactants on the water absorption of AASC specimens with the number of freeze-thaw cycles were plotted with the line chart shown in the figure, as shown in Figure 7.

From Figure 7, the water absorption of all groups of specimens increases with the increase of the number of freeze-thaw cycles. The water absorption rate of AASC without surfactants increased to 1.56 % at 20 times of freeze-thaw. Except for SA4 and SA5, the water absorption rate of the other specimens with surfactants was basically below 1.56 %. The water absorption rate of TS1 after 28 freeze-thaw cycles was as low as 1.45 %, which was lower than that of M0 group. This shows that the appropriate number of surfactants can reduce the water absorption of AASC, and the effect of 0.01 % TS is the best. The water absorption rate of AASC is the lowest when the content of SDS is 0.07 %, and the water absorption rate after 28 freeze-thaw cycles is 1.66 %. The water absorption rate of AASC is the lowest when the content of SA is 0.05 %, and the water absorption rate after 24 freeze-thaw cycles is 1.95 %. The water absorption rate of AASC is the lowest when the content of TS is 0.01 %, and the water absorption rate after 28 freeze-thaw cycles is 1.45 %.

3.6 Micro-analysis

3.6.1 SEM

In this part, the microstructure of M0 group and TS1 group was analyzed by scanning electron microscopy. The microscopic appearance at different magnifications is shown in Figure 8.

From Figure 8(a) and (b), the C-(A)-S-H gel on the surface of M0 group overlaps with each other and the structure is dense, forming a relatively complete whole. Moreover, the unreacted slag particles are basically not found, indicating that the hydration reaction of the slag particles is relatively complete. However, there are many cracks and holes. It is this porous and multi-crack structure that leads to poor frost resistance of M0 group specimens.

From Figure 9, there are many holes in the AASC after the incorporation of TS, but most of them are closed uniform holes, which can avoid the connection of the internal holes of the AASC. In addition, the introduced bubbles can reduce the pressure of freeze-thaw damage on the capillary wall and improve the ability of AASC to resist freeze-thaw damage. It can be observed that the surface without holes is relatively flat, the hydration products are dense, a large number of C-(A)-S-H gels are lapped together, and the structure is dense. This is the main reason why the frost resistance of AASC is better than that of M0 group after adding TS surfactants.

3.6.2 MIP

The hole structure has a crucial influence on the frost resistance of concrete. The size, shape and distribution of holes affect the frost resistance of AASC. Therefore, the samples of M0 and TS1 were prepared, and the mercury

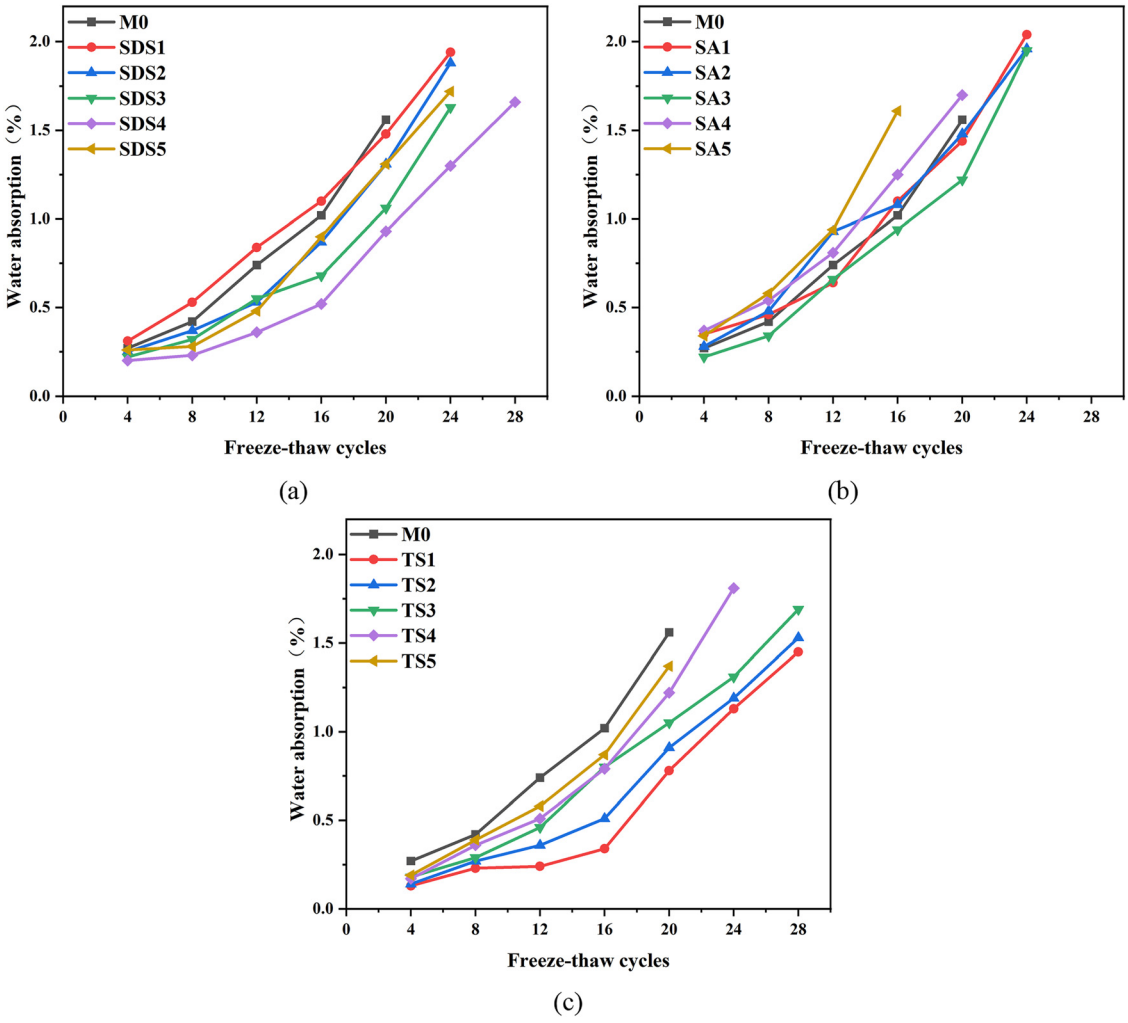

Figure 7: Water absorption rate under different freeze-thaw cycles.

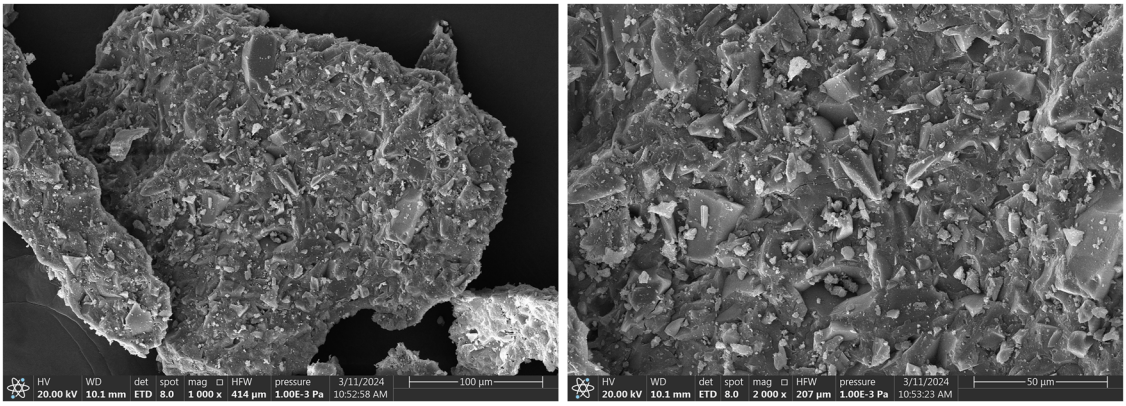

Figure 8: Microstructure analysis of M0 group.

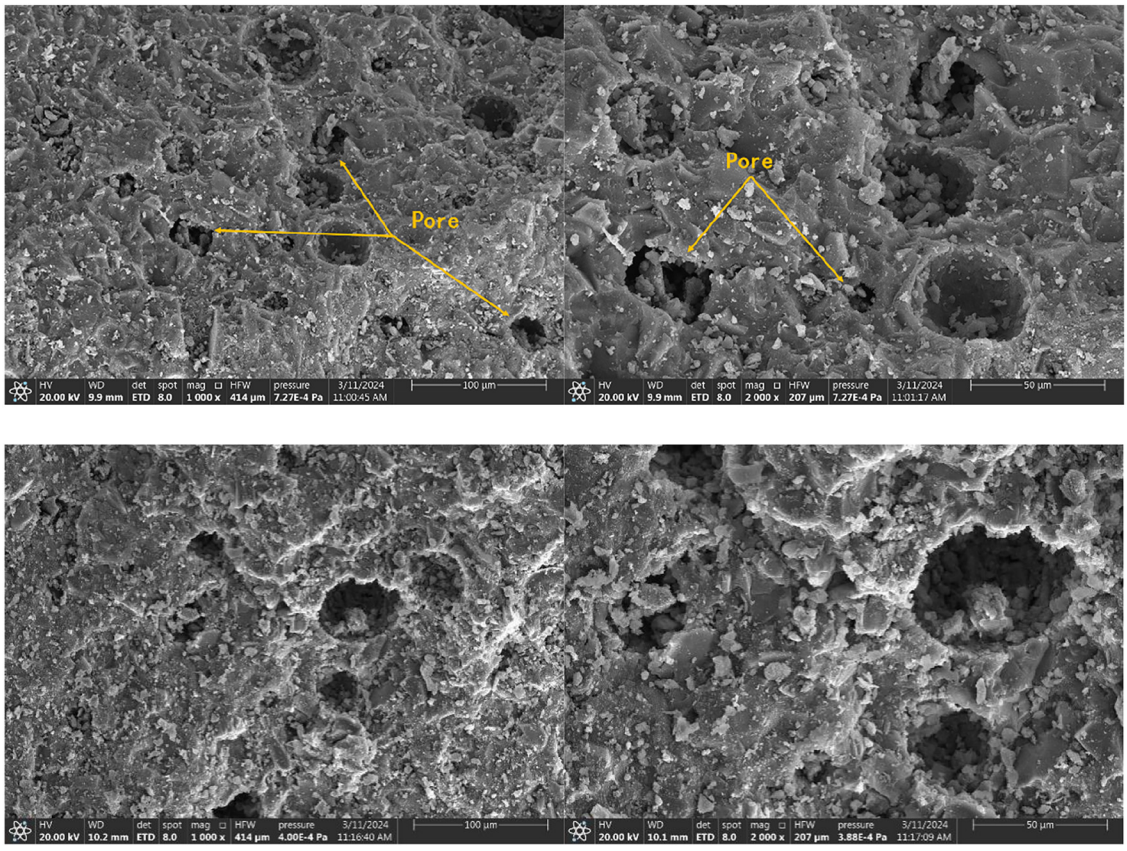

Figure 9: Microstructure analysis of TS1 group.

Table 3: Hole structure parameters.

Mix Id	Total porosity (%)	Total hole volume (mL/g)	Max hole size (nm)	Average hole diameter (nm)
M0	15.18	0.0205	40.30	26.43
TS1	17.75	0.0339	29.17	13.67

intrusion test was carried out to analyze the mechanism of hole structure affecting the frost resistance of AASC. The hole structure parameters of each group are shown in Table 3, and the hole size distribution differential curve is shown in the figure.

From Table 3, after adding TS surfactants, the total porosity of AASC increases, but its total hole volume, most probable hole size and average hole size decrease. The TS surfactants can form tiny bubbles in the AASC, which will disperse in the concrete and leave tiny holes. As the hydration reaction progresses, these bubbles will remain in the concrete, so the total porosity and total hole volume of the TS1 group samples increase. For the M0 group of samples, the most probable hole size is 40.30 nm. After adding TS surfactants, the most probable hole sizes are 29.17 nm and 32.43 nm, respectively, and the most probable hole sizes are reduced by 27.62 % and 19.52 %, respectively. Therefore, the hole connectivity becomes worse, the hole volume becomes finer, and the ability to resist freeze-thaw cycle is enhanced. The average hole size of the samples in the M0 group was 26.43 nm. After adding TS surfactants, the average hole size was 13.67 nm and 22.91 nm, respectively, which decreased by 49.04 % and 13.32 %, respectively. The decrease of average hole size showed that the number of small holes increased and the number of large holes decreased, so its ability to resist freeze-thaw cycle was enhanced [41, 42].

From Figure 10, the logarithmic differential mercury intake curve of the M0 group of samples has multiple peaks and is distributed in different hole size intervals. The hole size can be divided into macroholes (>103 nm), capillary holes (102–103 nm), transition holes (10–100 nm), and gel holes (<10 nm), according to the hole size of concrete. After the incorporation of TS surfactants, the peaks at the macroholes are significantly reduced, and the peaks are mainly concentrated in the transition holes and gel holes. The specific aperture distribution ratio is shown in Table 4.

The hole size of concrete is divided into four types: multi-hazard holes (>200 nm), harmful holes (50–200 nm),

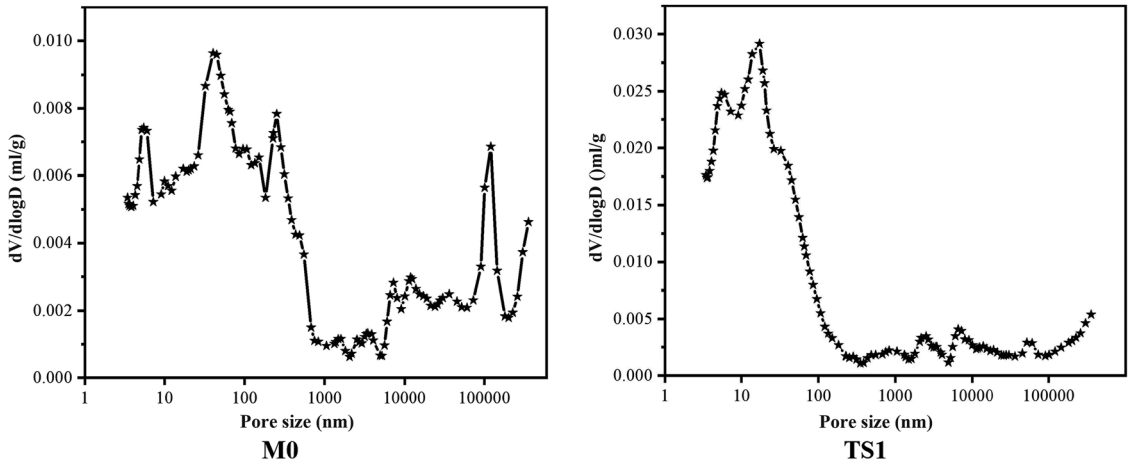

Figure 10: Logarithmic differential mercury intake curve diagram.

Table 4: Hole size ratio.

Mix Id	Hole size distribution (%)			
	<20 nm	20–50 nm	50–200 nm	>200 nm
M0	21.51	28.36	25.74	24.39
TS1	38.35	35.42	15.18	11.09

less harmful holes (20–50 nm), and harmless holes (<20 nm) according to the influence of hole size on frost resistance [43]. The proportion of multiple multi-hazard holes, harmful holes, less harmful holes and harmless holes in the M0 group was 24.39 %, 25.74 %, 28.36 % and 21.51 %, respectively. It can be seen that the proportion of harmless holes is the highest, followed by less harmful holes, which is the reason for the poor frost resistance of the M0 group. After adding TS surfactants, the proportion of harmless holes and less harmful holes in AASC increased, and the proportion of multi-hazard holes and harmful holes decreased. Compared with the M0 group, the proportion of multi-hazard holes and harmful holes in the TS1 group decreased by 54.53 % and 41.03 % respectively, and the proportion of less harmful holes and harmless holes increased by 24.89 % and 78.29 % respectively. The internal hole structure of AASC was optimized, so its frost resistance was better.

According to the corresponding references, TS are composed of hydrophilic sugar chains and have amphiphilic structures, which can form more stable micelles and interfacial membranes. Its rigid triterpenoid skeleton may enhance the order of molecular arrangement and improve the mechanical strength of the interfacial film. In contrast, the micelles and interfacial membranes formed by SDS and SA have low mechanical stability. TS are stable in alkaline or neutral environment, while carboxylates of SA are easy to react with high-valent metal ions (such as Ca^{2+}) to precipitate, and SDS is easy to fail under high ionic strength [30–32].

Based on the AASC compressive strength test and MIP test results presented in Section 3.4, the 28-day compressive strength of the M0 group was measured at 49.7 MPa. After undergoing a freeze-thaw cycle, the compressive strength decreased to 38 MPa, resulting in a compressive strength loss rate of 23.5 %. In contrast, the TS1 group exhibited a 28-day compressive strength of 47.4 MPa, with a post-freeze-thaw compressive strength of 42.4 MPa and a compressive strength loss rate of 10.5 %. The porosity of the M0 group was found to be 15.18 %, with an average hole size of 26.43 nm. For the TS1 group, the porosity increased to 17.75 %, while the average hole size decreased to 13.67 nm. This indicates that as the porosity increases, the average pore diameter decreases, the loss rate of compressive strength reduces, and the frost resistance of the concrete improves.

4 Conclusions

Based on the study of the effects of different dosages of surfactants on the frost resistance of AASC, the following conclusions were made:

1) The incorporation of surfactants will reduce the initial setting time of AASC, but increase its final setting time. Among them, TS surfactant has the least effect on the 28d compressive strength of AASC. When the content is 0.01 %, the 28d compressive strength is only reduced by 4.6 %.
2) With the increase of the dosage of the three surfactants, when the SDS content was 0.07 %, the frost resistance of AASC is the best. When the dosage of SA is 0.05 %, the frost resistance of AASC is the best. When the dosage of

TS is 0.01 %, the frost resistance of AASC is the best. TS had the best effect on improving the frost resistance of AASC, followed by SDS, and SA had the worst effect.

3) When the surfactant is not added, the number of cracks and harmful macroholes in AASC is more, and the cracks in the interfacial transition zone are narrow and long, and there are many cracks. It can be clearly observed that uniform and closed microbubbles are introduced into AASC after adding surfactants. The most probable hole size and average hole size decreased, and the proportion of harmful holes and multi-harmful holes decreased. These microbubbles prevented the connection of holes, inhibited the formation of harmful macroholes, and improved the frost resistance of AASC.

Funding information: This work was supported by Shandong Provincial Natural Science Foundation (ZR2022ME133), and National Natural Science Foundation of China (51908342).

Author contribution: Xuekun Jiang: writing – original draft, investigation, methodology, formal analysis, data curation, conceptualization. Zhirong Jia: writing – review and editing, resources, formal analysis, funding acquisition. Yaoxi Han: writing – review and editing methodology, conceptualization. Xuejing Wang: writing – review and editing, formal analysis, data curation, conceptualization. Xinyu Yang: writing – review and editing, supervision, methodology. Jiantong Wu: writing – review and editing, conceptualization. All authors have accepted responsibility for the entire content of this manuscript and approved its submission.

Conflict of interest: The authors state no conflict of interest.

Data availability statement: The datasets generated and/or analysed during the current study are available from the corresponding author on reasonable request.

References

1. Zhao H, Jiang K, Yang R, Tang Y, Liu J. Experimental and theoretical analysis on coupled effect of hydration, temperature and humidity in early-age cement-based materials. Int J Heat Mass Tran 2020;146: 118784.
2. Gartner E. Industrially interesting approaches to "low-CO_2" cements. Cem Concr Res 2004;34:1489–98.
3. Tong S, Yuqi Z, Qiang WJ. Recent advances in chemical admixtures for improving the workability of alkali-activated slag-based material systems. Constr Build Mater 2021;272:121647.
4. Zhao Z, Wang S, Ren J, Wang Y, Wang C. Fatigue characteristics and prediction of cement-stabilized cold recycled mixture with road-milling materials considering recycled aggregate composition. Constr Build Mater 2021;301:124122.
5. Awoyera P, Adesina A. A critical review on application of alkali activated slag as a sustainable composite binder. Case Stud Constr Mater 2019; 11:e00268.
6. Luukkonen T, Abdollahnejad Z, Yliniemi J, Kinnunen P, Illikainen M. One-part alkali-activated materials: a review. Cem Concr Res 2018;103: 21–34.
7. Provis JL. Alkali-activated materials. Cem Concr Res 2018;114:40–8.
8. Provis JL, Palomo A, Shi C. Advances in understanding alkali-activated materials. Cem Concr Res 2015;78:110–25.
9. Duxson P, Fernández-Jiménez A, Provis JL, Lukey GC, Palomo A, Van Deventer JS. Geopolymer technology: the current state of the art. J Mater Sci 2007;42:2917–33.
10. Marvila MT, Azevedo ARG, Vieira CMF. Reaction mechanisms of alkali-activated materials. Rev IBRACON Estrut Mater 2021;14:e14309.
11. Yang Z, Tang W, Zhang D, Zhang J, Wang K, Zhao Z. Hydration mechanism of alkali-activated cementitious materials entirely prepared by solid wastes. J Build Eng 2024;97:110921.
12. Su C, Zhang J, Ding Y. Research on reactivity evaluation and micro-mechanism of various solid waste powders for alkali-activated cementitious materials. Constr Build Mater 2024;411:134374.
13. Zhao C, Wang Z, Zhu Z, Guo Q, Wu X, Zhao R. Research on different types of fiber reinforced concrete in recent years: an overview. Constr Build Mater 2023;365:130075.
14. Rodrigue A, Duchesne J, Fournier B, Bissonnette B. Frost resistance of alkali-activated combined slag and fly ash concrete cured at ambient temperature. ACI Mater J 2022;119:3–13.
15. Zheng X, Liu F, Luo T, Duan Y, Yi Y, Hua C. Study on durability and hole characteristics of concrete under salt freezing environment. Materials 2021;14:7228.
16. Shang HS, Yi TH. Freeze-thaw durability of air-entrained concrete. Sci World J 2013;2013:650791.
17. Ke G, Zhang J, Tian B, Wang J. Characteristic analysis of concrete air entraining agents in different media. Cem Concr Res 2020;135:106142.
18. He J, Gao Q, Song X, Bu X, He J. Effect of foaming agent on physical and mechanical properties of alkali-activated slag foamed concrete. Constr Build Mater 2019;226:280–7.
19. Sun Q, Wei X, Li T, Zhang L. Strengthening behavior of cemented paste backfill using alkali-activated slag binders and bottom ash based on the response surface method. Materials 2020;13:855.
20. Chen Y, Al-Neshawy F, Punkki J. Investigation on the effect of entrained air on hole structure in hardened concrete using MIP. Constr Build Mater 2021;292:123441.
21. Li M, Zhou X, Zhao J, Qu S, Wang P, Li G. Preliminary exploration of a novel high-performance air entraining agent based on sodium dodecyl sulfate added self-made fluorocarbon surfactant. Constr Build Mater 2023;370:130564.
22. Peng GF, Ma Q, Hu HM, Gao R, Yao QF, Liu YF. The effects of air entrainment and pozzolans on frost resistance of 50-60 MPa grade concrete. Constr Build Mater 2007;21:1034–9.
23. Ouyang X, Guo Y, Qiu X. The feasibility of synthetic surfactant as an air entraining agent for the cement matrix. Constr Build Mater 2008;22: 1774–9.
24. Łaźniewska-Piekarczyk B. The type of air-entraining and viscosity modifying admixtures and porosity and frost durability of high performance self-compacting concrete. Constr Build Mater 2013;40: 659–71.
25. Deo O, Neithalath N. Compressive behavior of pervious concretes and a quantification of the influence of random hole structure features. Mater Sci Eng A 2010;528:402–12.

26. Tunstall LE, Ley MT, Scherer GW. Air entraining admixtures: mechanisms, evaluations, and interactions. Cem Concr Res 2021;150:106557.
27. Feng T, Yang H, Zhang J, Zong C. Applicability of cationic surfactants, anionic surfactants, and nonionic surfactants as foaming agents for foamed concrete: surface activity, foamability, and interaction with cement. J Sustain Cem-Based Mater 2024;13:1330–47.
28. Chen J, Qiao M, Gao N, Ran Q, Wu J, Shan G, et al. Cationic oligomeric surfactants as novel air entraining agents for concrete. Colloids Surf A Physicochem Eng Asp 2018;538:686–93.
29. Yan DM, Ruan SQ, Chen SK, Liu Y, Tian Y, Wang HL, et al. Effects and mechanisms of surfactants on physical properties and microstructures of metakaolin-based geopolymer. J Zhejiang Univ - Sci 2021;22:130–46.
30. Sahu SS, Gandhi ISR. Studies on influence of characteristics of surfactant and foam on foam concrete behaviour. J Build Eng 2021;40:102333.
31. Zhang J, Qi Y, Lv T, Niu X, Tai B. Effects of sodium dodecyl sulfate on nano carbon black-filled cement paste: performance and microstructure. J Mater Res Technol 2023;24:1706–15.
32. Wu J. Study on the effect of different air-entraining agents on the properties of concrete. E3S Web Conf 2025;618:02001.
33. Li Q, Ge Y, Yang W. Effect of sodium sulfate and sodium nitrite on air-void system in air-entrained concrete. Mag Concr Res 2016;68:1200–9.
34. Sun C, Zhu Y, Guo J, Zhang Y, Sun G. Effects of foaming agent type on the workability, drying shrinkage, frost resistance and hole distribution of foamed concrete. Constr Build Mater 2018;186:833–9.
35. Hu J, Zhao F, Kuang Y, Yang D, Zheng M, Zhao L. Microscopic characteristics of the action of an air entraining agent on cemented paste backfill holes. Alexandria Eng J 2020;59:1583–93.
36. Yang Q, Zhu P, Wu X, Huang S. Properties of concrete with a new type of saponin air-entraining agent. Cem Concr Res 2000;30:1313–7.
37. Maglad AM, Mydin MAO, Datta SD, Abbood IS, Tayeh BA. Impact of anionic surfactant-based foaming agents on the properties of lightweight foamed concrete. Constr Build Mater 2024;438:137119.
38. Wang X, Wu Y, Li X, Li Y, Tang W, Dan J, et al. Effect of triterpenoid saponins as foaming agent on mechanical properties of geopolymer foam concrete. Materials 2024;17:3921.
39. Zhou X, Bai S, Zhou X, Zhang Y, Ding Q. Effect of foaming characteristics of air entrained agents on mechanical properties and hole structures of cement-based materials in plateau mountainous regions. J Build Eng 2024;91:109590.
40. Hu JH, Kuang Y, Zhou T, Zhao F. Influence of air entraining agent on strength and microstructure properties of cemented paste backfill. IEEE Access 2019;7:140899–907.
41. Turkoglu M, Bayraktar OY, Benli A, Kaplan G. Effect of cement clinker type, curing regime and activator dosage on the performance of one-part alkali-activated hybrid slag/clinker composites. J Build Eng 2023;68:106164.
42. Bayraktar OY, Kaplan G, Benli A. The effect of recycled fine aggregates treated as washed, less washed and unwashed on the mechanical and durability characteristics of concrete under $MgSO_4$ and freeze-thaw cycles. J Build Eng 2022;45:103924.
43. Zhao M, Dong W. Grey relativity correlations between the hole structures and compressive strength of Aeolian sand concrete undergoing carbonation and freeze-thaw cycles. J Build Eng 2023;76:107515.